Engineering Fracture Mechanics 224 (2020) 106784

Contents lists available at ScienceDirect

Engineering Fracture Mechanics

journal homepage: www.elsevier.com/locate/engfracmech

A probabilistic framework to define the design stress and acceptable defects under combined-cycle fatigue conditions

L. Patriarca[a,*], S. Beretta[a], S. Foletti[a], A. Riva[b], S. Parodi[b]

[a] Politecnico di Milano, Department of Mechanical Engineering, via La Masa 1, 20156 Milano, Italy
[b] Ansaldo Energia, Via N. Lorenzi, 8, Genova, Italy

ARTICLE INFO

Keywords:
Combined high and low cycle fatigue
Defect tolerance
Reliability
Probabilistic threshold model

ABSTRACT

Probabilistic routines are necessary to determine the permissible design stress when the operational conditions of traditional gas turbines are further challenged to reach higher performances in terms of flexibility. This paper focuses on the definition of a probabilistic tool aimed to simulate the damage development under combined high and low cycle fatigue conditions considering the stochastic nature of some of the variables introduced in the model. The variables considered in the present study are the long crack threshold $\Delta K_{th,LC}$ and the slope of the crack growth law C in the so-called Paris region, the endurance limit $\Delta\sigma_{w0}$ and the variability of the applied stress as it cannot be considered a fixed variable in the complex loading scenario of gas turbines. A broad experimental campaign was performed to characterize the material properties in terms of short and long crack resistance under constant and combined cyclic conditions. The data were used to define the average and variance of the materials parameters to feed Montecarlo simulations and, at a target probability of failure, establish the design stress. This work points to determine safety margins which strictly depend on the natural variability of the variables that govern the damage accumulation in the mechanical component.

1. Introduction

The present paper describes the research activity performed in the framework of the European project Flexturbine which mainly aimed to develop knowledge to allow high superior performances in flexible operation of gas turbines. In general, gas turbines experience very complex loading conditions which include both mechanical and thermal stresses, as well as extreme environmental conditions (corrosion, erosion, fluid-structure interaction at high temperatures, impacts with foreigner objects, etc) which further increase the level of complexity of the design process. In fact, the combination of these extreme loading and environmental conditions determine different potential types of damage that successively originates the component failure. The present manuscript focuses on the development of a design procedure for the safety assessment of a crack/defect in the complex loading scenario of the combined high and low cycle fatigue (CCF) conditions. The typical CCF cycle is defined by a major load cycle that corresponds to the start-up cycle of the gas turbine (stress ratio $R = 0$) and the superposition of secondary stresses originated by, for example, blade vibrations ($R > 0$). The material under investigation is the X5CrNiCuNb16-4 precipitation hardening martensitic stainless steel typically used in components of heavy-duty gas turbines.

The definition of the allowable stress for critical mechanical components is a key aspect in the design process. For gas turbine applications, the definition of the design stress is required to account for a certain degree of conservatism to avoid catastrophic

* Corresponding author.
E-mail address: luca.patriarca@polimi.it (L. Patriarca).

https://doi.org/10.1016/j.engfracmech.2019.106784
Received 29 March 2019; Received in revised form 25 September 2019; Accepted 14 November 2019
Available online 29 November 2019

Nomenclature

a_{crit}	critical crack length
$\sqrt{area}$	equivalent crack length
$\sqrt{area_0}$	El-Haddad parameter
Y	geometric factor
R	load ratio
N	number of cycles
da/dN	crack growth rate
σ_y	monotonic yield stress
σ_F	flow stress
σ_a	stress amplitude
σ_m	mean stress
$\Delta\sigma_{w0}$	endurance limit for smooth specimens
$\Delta\sigma_w$	endurance limit for short-cracked specimens
K	stress intensity factor
K_C	fracture toughness
K_{max}	maximum stress intensity factor
K_{op}	stress intensity factor at crack opening
ΔK	range of stress intensity factor
$\Delta K_{th,LC}$	long crack threshold range
C, n, p, q	material parameters of the NASGRO equation
f	crack closure parameter
A_0, A_1, A_2, A_3	parameters of Newman's crack closure equation
α	constraint factor
ΔK_1	long crack threshold for $R \rightarrow 1$
ΔK_1^*	short crack-corrected ΔK_1
C_{th}^p	parameter of the NASGRO equation for positive long crack thresholds
C_{th}^n	parameter of the NASGRO equation for negative long crack thresholds
σ	standard deviation
ρ	coefficient of correlation
P_f	probability of failure
CV	coefficient of variance
d	mean grain size
ΔS	applied stress range on the component
ΔS_0	design stress range for the Scenario 0
$\Delta S_{0,det}$	deterministic design stress range for the Scenario 0
ΔS_1	design stress range for the Scenario 1
ΔS_2	design stress range for the Scenario 2

failures. To define a proper safety factor, different approaches can be adopted in the case of gas turbine components [1]. In the life-to-first-crack approach the failure is defined once reaching a surface crack length of 0.75 mm, the design curve being defined according the -3σ methodology [2]. This approach does not consider the maximum allowable defect which, in some cases, can be much longer than 0.75 mm leading to very conservative designs. More refined approaches, for example applied to turbine disks, consider the component life in terms of propagation of manufacturing defects under service conditions and mission profiles [3–6].

The loading considered for the compressor blades can be synthetically defined as the combination of a major loading cycle representing the start-up cycle at load ratio R = 0 and the secondary loading cycles (generally specified at a positive load ratio R>0) induced, for example, by the blade vibrations. According to a damage tolerance design, both the stress ranges of the major cycle (R = 0) and the one induced by the blade vibration (R>0) are required to be lower than the corresponding allowable (design) stress range. The designer can safely assess the allowable stress ranges as the stresses which do not induce a defect (or a crack) with a specified dimension to propagate accounting for a proper safety factor. One tool to implement this design strategy based on non-propagating cracks is the adoption of the so-called Kitagawa-Takahashi diagram [7]. This diagram simply projects the endurance limit as a function of the defect size. Two limit conditions are observed: (i) when the crack size tends to zero the endurance limit corresponds to the one determined on the smooth specimens $\Delta\sigma_{w0}$, while (ii) when the crack size is large the endurance limit can be defined according to the long crack threshold condition $\Delta K_{th,LC}$. Between these two limits, short cracks can propagate with stresses below the threshold conditions determined by the endurance limit and the long crack threshold [8]. It is then important firstly to calibrate a model which properly describes the change of the endurance limit from the condition of ideal zero defect towards the long crack condition and through the short crack regime. However, the calibration of this model is not sufficient to define an efficient design strategy. As an example, let's consider a severe service of 30 year (with two start-ups per day) leading to a target gas turbine life of N = 18,000 cycles. The adoption of the Kitagawa-Takahashi diagram to predict the allowable design stress for the major loading cycles (R = 0) for such limited number of cycles might lead to an over-conservative design. To avoid this over-conservatism, it is possible to consider a stress level which allows a certain crack advancement induced by the major loading cycles. More specifically, to introduce the effect of the major loading cycles, two possibilities were explored and discussed in the paper. In the first (hereinafter referenced as Design scenario 1) the crack advancement produced by the major loading cycles (startup cycles) was initially calculated (neglecting the vibrational cycles) and the advanced crack was successively considered for the definition of the design stress adopting the Kitagawa-Takahashi diagram for the vibrational stresses. In the second scenario (Design scenario 2), a complete crack propagation calculation considering both the major and vibrational loading cycles in the correct sequence was performed. As it will be shown in the manuscript, the first methodology is a simplified scenario but still provides a reasonable approximation of the second approach which is more computationally demanding, unless strictly related with the real loading sequence.

The aim of this paper is a detailed analysis of the damage mechanisms induced according the combined-cycle fatigue conditions, in order to determine an accurate analysis of the definition of the design stress in probabilistic terms. In the first part of this work, a detailed experimental campaign was performed to characterize the crack growth mechanisms and the threshold model able to represent the CCF conditions of the gas turbine. In the second part of the paper, a probabilistic framework aimed to define the design stress is presented.

Firstly, the experimental scatter of the threshold conditions for long and short cracks was accounted for and quantified. In particular, from the experiments, the variability of the long crack threshold $\Delta K_{th,LC}$ was considered as a function of the load ratio. The endurance limit for smooth specimens $\Delta\sigma_{w0}$ was also considered to be a stochastic variable. Montecarlo simulations were then

performed to generate statistical Kitagawa-Takahashi diagrams according the anlaytical model of El-Haddad [9] with different statistical models [10–12]. An important aspect of this analysis, which is discussed in the manuscript, is the level of correlation between $\Delta K_{th,LC}$ and $\Delta\sigma_{w0}$ with the latter strictly related with the yield stress σ_y based on several sources for different materials [13–15].

The probabilistic model was also calibrated to account for the crack growth. The NASGRO model [16] was adopted to account for both the threshold and Paris regions of the ΔK versus da/dN data. The scatter of the experimental data was used to define the variability of the crack growth rates. The crack growth model was used to simulate the crack advancement starting from a defect/crack originated by the martensitic microstructure itself or by local damage produced, for example, by foreign objects. An additional source of variability was introduced to account for the stress induced by the vibration cycles as there are uncertainties in estimating this value.

To summarize, the probabilistic model presented in this study is capable of simulating the crack propagation and establish the endurance limit condition for short cracks for the CCF regime. The stochastic variables used are (i) the stress induced by the vibration cycles and three materials properties: (ii) the long crack SIF range $\Delta K_{th,LC}$, (iii) the endurance limit for smooth specimens $\Delta\sigma_{w0}$ and (iv) the constant C of the NASGRO equation used to calculate the crack growth rates. The model was used to determine a map of permissible design stresses for three design scenario which are deeply discussed in the following.

2. Experiments

2.1. Material and specimens

The present X5CrNiCuNb16-4 alloy is a precipitation hardening (PH) martensitic stainless steel employed in compressor blades. The hardening effect is caused by the ϵ-Cu particles which are highly dispersed in the martensite matrix. Besides, the δ-ferrite is present and its amount is strongly influenced by the heat treatment. These PH steels are generally used in environments where a level of corrosion resistance comparable to that of austenitic grades is needed, but in applications that require higher strength and hardness than the austenitic grades can provide. For these reasons, the X5CrNiCuNb16-4 is employed in early stage compressor blades ensuring high performances. Furthermore, for the X5CrNiCuNb16-4 alloy, hardening is activated through the addition by Cu and Nb. The strengthening process is implemented in three steps. In the first, a solution treatment is adopted to favor the machining. Successively, quenching is performed to obtain a supersaturated solid solution resulting in a fine grain size. At the end, aging is aimed to decompose the supersaturated solid solution into small precipitate clusters resulting in an hardness increment. The resulting microstructure is shown in Fig. 1 and it is characterized by a lamellar structure with fine martensitic laths. Small carbides are dispersed at primary grain boundary and between the martensitic laths. The figure also indicates that the lamellar grains might be prompted to facilitate crack nucleation, in this case the dimension to be considered in the damage tolerance approach is the average dimension of this lamellar structures.

The specimens adopted in the present study are reported in Fig. 2 and a brief summary of the tests implemented according the specimen geometries is given in Table 1. The cylindrical geometry (Fig. 2a) was chosen to derive the endurance limits $\Delta\sigma_{w0}$ for the load ratio $R = 0$ and $R = 0.5$. The specimen length was 110 mm and the diameter of the cross-section was 8 mm. A total number of 14 specimens were used to define the stair-case sequences for the fatigue tests. The same specimen geometry was also adopted for deriving the endurance limit in the presence of a micro-notch $\Delta\sigma_w$ (Fig. 2b). The micro-notches were obtained by electrical discharge machining (EDM) into a semi-circular shape with radius of 150 μm resulting in an equivalent $\sqrt{area} = 187$ μm, i. e. the Murakami's parameter which characterizes an equivalent length of a small crack or defect with a random geometry [17]. Also for this type of tests the number of specimens adopted was 14 and the same load ratios $R = 0$ and $R = 0.5$ were investigated. A third type of specimen geometry was specifically designed to enhance the superficial crack propagation detection. For this purpose, two flattened surfaces were machined by EDM to allow a precise measurement of the crack advancement (Fig. 2c). The diameter of the cross-section was

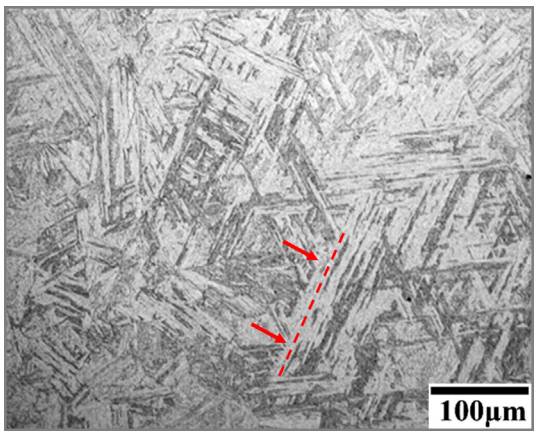

Fig. 1. Lamellar microstructure of the present X5CrNiCuNb16-4.

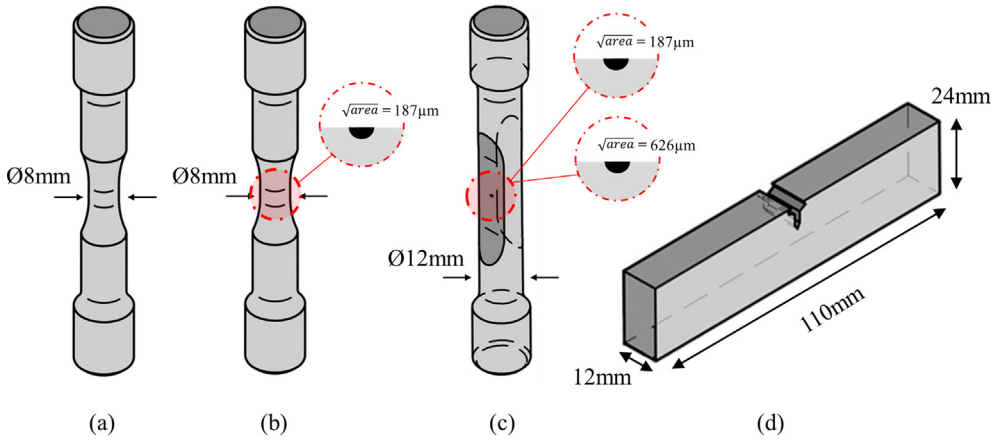

Fig. 2. Specimen geometries adopted in the present study: (a) smooth cylindrical to perform endurance limit tests; (b) micro-notched cylindrical with micro-notch dimension $\sqrt{area_0}$ = 187 μm; (c) micro-notched flattened cylindrical to perform CCF short crack propagation tests: two micro-notch sizes were investigated $\sqrt{area}$ = 187 μm and $\sqrt{area}$ = 626 μm; (d) the single-edge notched bending geometry to perform long crack growth tests.

Table 1
Experimental planning of the present study.

Specimen geometry	Test target	Crack type	Load ratio R	Tests
Fig. 2a	Endurance limit $\Delta\sigma_{w0}$	No	0; 0.5	14
Fig. 2b	Endurance limit with short-crack $\Delta\sigma_w$	Short-crack $\sqrt{area}$ = 187 μm	0; 0.5	14
Fig. 2c	Crack growth under CCF	Short-crack $\sqrt{area}$ = 187 μm	0; 0.5	3
		Long-crack $\sqrt{area}$ = 626 μm	0; 0.5	1
Fig. 2d	Long crack threshold $\Delta K_{th,LC}$	Long crack	0; 0.5	9

12 mm and the distance between the two parallel surfaces was 7 mm. For these tests, a total number of 4 specimens were used. The tests were performed under CCF loading with the major loading cycle at R = 0 and the high frequency cycles representing the vibrational stress at R = 0.5. These tests were implemented to simulate the short-crack effect under CCF conditions. Specifically, 3 specimens were machined according a micro-notch with $\sqrt{area}$ = 187 μm. This defect size was chosen according the dimension of a potential defect originated from the material microstructure. Additionally, one test was performed on a specimen with a machined micro-notch of $\sqrt{area}$ = 626 μm to simulate the damage induced by the impact of a foreigner object. Finally, the single-edge notched bending (SEB) specimen (Fig. 2d) was used to measure the long crack growth rates and the long crack thresholds in terms of range of stress intensity factor (SIF) $\Delta K_{th,LC}$. The SEB specimens geometry was 110 mm length, 24 mm width and 12 mm thickness, while the notch length was 6.5 mm.

Prior to testing, the cylindrical and flattened specimens (Fig. 2a–c) were electro-polished to remove the high residual stresses resulting from machining using a solution of 94% of acetic acid and 6% perchloric acid. To be noted, the electro-polishing was performed before the machining of the micro-notches. The average thickness of the layer removed was approximately 44 μm. The electro-polishing also determined a very smooth surface which satisfied the requirements of the ASTM E466-15 standard on the maximum longitudinal surface roughness to be lower than 0.2 μm [18]. Table 2 reports the residual stress measurements performed before and after the electro-polishing by means of an AST X-Stress 3000 portable X-ray diffractometer.

Most of the experiments on the cylindrical specimens (Fig. 2a–c) were performed under a uniaxial resonant Rumul machine with maximum load capacity of 100kN. Some tests under CCF were conducted on a servo-hydraulic MTS machine as the small number of cycles at R = 0.5. The crack propagation tests were performed on a resonant Rumul bending machine equipped with a Fractomat unit used to measure the crack advancements. The Fractomat unit is connected with two resistance foils glued on the specimen surfaces in proximity of the notch tip. During the tests, the resistance foils fracture following the crack advancement. The crack propagation induces a change of the electrical resistance of the foils which is calibrated with the crack length. To be noted, the crack length is

Table 2
Residual stress measurements performed to calibrate the electro-polishing procedure.

Specimen	$\sigma_{0°}$ (MPa)	$\sigma_{45°}$ (MPa)	$\sigma_{90°}$ (MPa)	σ_I (MPa)	σ_{II} (MPa)
As-manufactured	−454.2	399.2	−398.2	−387.3	−465.2
Electropolished	−99.5	−131	−0.6	44.8	−144.9

measured, with this technique, on the fracture surfaces. After the tests, each specimen was broken to analyze the fracture surfaces. The final crack front was then used to eventually correct the crack length measurements.

2.2. Endurance limits and short-crack effect

The endurance limits were measured through two short stair-case sequences on the smooth cylindrical specimens at two load ratios, R = 0 and R = 0.5. A total number of 14 specimens were tested, in particular 7 specimens for each load ratio.The run-outs were considered the specimens that survived for 10^7 cycles. The fatigue limit was then calculated according the modified stair case method provided in the ISO 12107 standard [19]. The experimental results (as failures and run-outs) are reported in Fig. 3 in terms of normalized stress amplitude values with respect to the yield stress σ_a/σ_y. Such diagram was defined according the FKM guideline [20]. For the load ratio under investigation, the experimental mean stress effect is consistent with the continuum yield line which shows that failures occur when the maximum stress of the fatigue cycles is higher than the yield stress. When the micro-notch is introduced, it is observed that there is a remarkable drop of the fatigue strength.

It is important to underline that the measurement of the endurance limits in the case of micro-notched specimens aims to experimentally define the resistance of the present alloy to small crack propagation. For this reason, all the micro-notched specimens were initially pre-cracked at a negative load ratio of −2.5. The negative load ratio enhances the crack nucleation and results in micro-cracks which are embedded in the compressive plastic region of the notch with the effect of minimizing the crack closure. The stress range adopted during the pre-cracking was selected according an initial stair-case procedure aimed to determine the failure and run-out stress levels at the load ratio −2.5. Successively, all the specimens were pre-cracked according the run-out stress level for a number of cycles of 10^7. This procedure guarantees that the successive tests at positive load ratio are effectively implemented on short-cracked specimens with limited initial crack closure. Following the pre-cracking procedure, the specimens were tested under a resonant loading frame. During the tests, the test frequency was continuously monitored and used to eventually stop the test to avoid the complete specimen failure. In fact, a propagating crack induces a change of the specimen stiffness which determines a change of the test frequency. The run-out condition (or, alternatively, the non propagating condition for the short crack) was then assured when two conditions were achieved: (i) the specimen did not fail; (ii) the test frequency did not change during the 10^7 cycles. An example of a non-propagating crack following a run-out test performed at R = 0 is shown in Fig. 4. In the micrograph, the bottom sides of the EDM micro-notch show two small cracks propagated in the plane of the specimen cross section. That confirms that the endurance limits detected for the micro-notched specimens refer to a small non-propagating crack.

The fatigue properties were derived to construct a proper analytical model which describes the variation of the endurance limit according a specific crack dimension represented in the so-called Kitagawa-Takahashi diagram [7]. To define an analytical equation several models have been proposed in literature, the El-Haddad model [9] can be readily used with a limited number of material properties: the endurance limit for smooth specimens $\Delta\sigma_{w0}$ and the long crack SIF threshold $\Delta K_{th,LC}$:

$$\Delta\sigma_w = \Delta\sigma_{w0}\sqrt{\frac{\sqrt{area_0}}{\sqrt{area}+\sqrt{area_0}}} \tag{1}$$

Eq. (1) is written considering the Murakami's equivalent crack length $\sqrt{area}$. The parameter $\sqrt{area_0}$ depends on the load ratio and it is defined as the crack size corresponding to the intersection between the horizontal line defining the endurance limit $\Delta\sigma_{w0}$ and the line defining the purely linear elastic fracture mechanics domain (dashed lines in Fig. 5) $\Delta K_{th,LC} = \Delta\sigma_w Y\sqrt{\pi\sqrt{area}}$. By substituting $\Delta\sigma_w = \Delta\sigma_{w0}$ one can easily find $\sqrt{area_0}$ as:

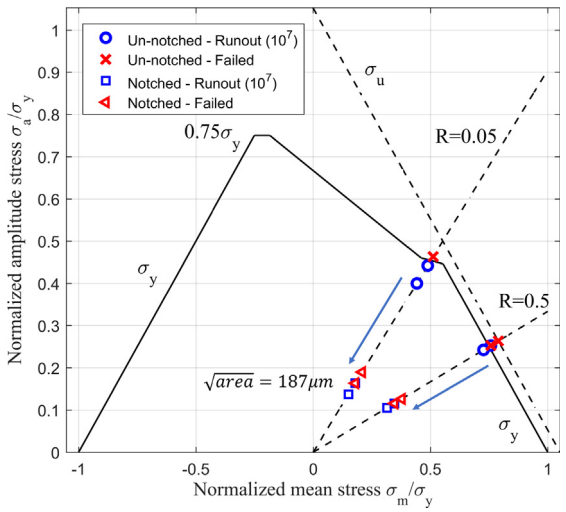

Fig. 3. Mean stress effect for the endurance limits determined on the smooth cylindrical specimens and on the micro-notched specimens ($\sqrt{area}$ = 187 μm). The endurance limits detected for the smooth specimens are well described by the yield limit condition.

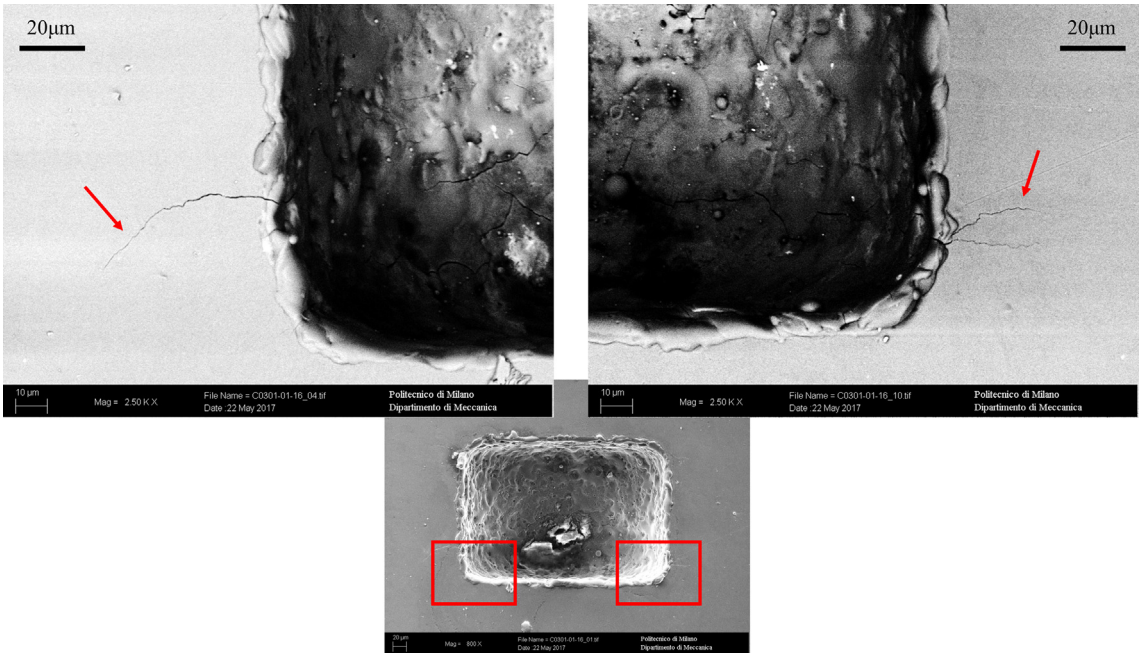

Fig. 4. Example of a non-propagating short crack for the tests performed on the micro-notched cylindrical specimens.

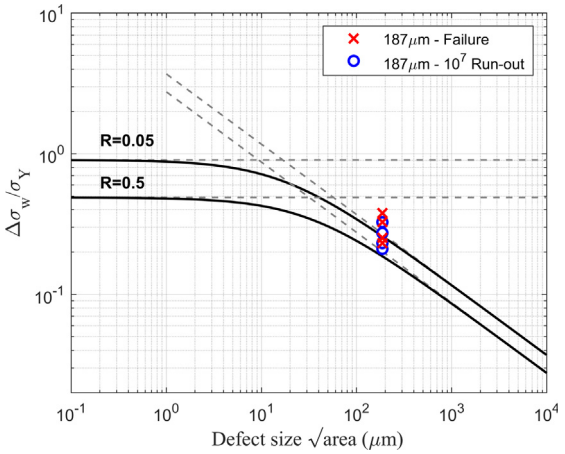

Fig. 5. Endurance limits for the micro-notched specimens and comparison with the El-Haddad model.

$$\sqrt{area_0} = \frac{1}{\pi}\left(\frac{\Delta K_{th,LC}}{Y\Delta\sigma_{w0}}\right)^2 \tag{2}$$

The parameter Y is a constant that depends on the specimen and crack geometry, in addition it depends on the definition of the crack size (a or $\sqrt{area}$). For the specimen geometry indicated in Fig. 2c, the specimen section can be approximated with a plate having a width of 12 mm and a thickness of 7 mm. The geometry factor for a semi-circular crack can be calculated with the classical Newman-Raju equation providing a value of approximately 0.732 from very small cracks to longer crack lengths (up to 1 mm)[21]. If $\sqrt{area}$ is adopted instead of a, for the same geometry, the parameter Y has to be used equal to 0.65. The same can be applied to a semi-circular surface crack for a round bar (specimen geometry depicted in Fig. 2a-b). Eq. (1) is represented with two continuum black lines representing the load ratio R = 0 and R = 0.5 in Fig. 5. The long crack SIF threshold values were experimentally measured and are introduced in the next section.

2.3. Long-crack behavior

In this section, the experimental results related to the long crack growth behavior are presented. The adopted SEB specimens (Fig. 2d) were initially pre-cracked in compression to generate an initial closure-free crack at the notch tip under a four-point-bending

set-up (for further details on the compression pre-cracking procedure see for example [22–24]). Following the pre-cracking, the specimens were subjected to an initial block of constant amplitude fatigue cycles at a fixed load ratio R. The aim of this initial step is the development of the crack closure and a stabilization of the crack growth rate at approximately $2{\cdot}10^{-9}$ m/cycles. Following this initial stabilization crack growth, the crack has typically advanced between 1 mm and 2 mm (depending on the load ratio). If the experiment targets to obtain the crack growth data in the so-called Paris region, the test is continued under the same constant amplitude fatigue cycles to further advance the crack and then increase the applied ΔK that increases according the square-root of the crack length. On the other side, if the requirement of the test is the determination of the $\Delta K_{th,LC}$, the test is performed under a load reduction procedure which is based upon a decrease of the applied load amplitude which generates a decrease of the applied ΔK. The decrease of the applied load has to be calibrated according the ASTM E647-15 standard to be sufficient to compensate the increment of ΔK with the crack advancement, and not too high to minimize the load history effects [25].

The summary of the crack growth data acquired are reported in Fig. 6 which includes a total of 6 experiments combining both increasing and decreasing ΔK. The blue points represent the crack growth data obtained at R = 0, while the red dots are those data obtained for the load ratio R = 0.5. The model which fits the crack growth rates is the Nasgro equation [16]:

$$\frac{da}{dN} = \underbrace{C\cdot\left[\left(\frac{1-f}{1-R}\right)\Delta K\right]^{n}}_{Region2}\cdot\frac{\overbrace{\left(1-\frac{\Delta K_{th,LC}}{\Delta K}\right)^{p}}^{Region1}}{\underbrace{\left(1-\frac{K_{max}}{K_c}\right)^{q}}_{Region3}} \tag{3}$$

The terms C, n, p and q are material parameters which are required to be fitted according the available experimental data. Region 1 indicated in Eq. (3) refers to the threshold region and the exponent p determines the shape of the knee in the descending part of the curve. Region 2 defines a linear relation (in the log-log scale) between ΔK and da/dN while region 3 describes the unstable crack propagation region (not considered in this study, q is then set to zero). The term f accounts for the level of crack closure and depends on the load ratio R, as well as the threshold $\Delta K_{th,LC}$. In the next section, further details are provided for the calculation and fitting of these terms, in particular for the implementation of the probabilistic methodology.

According to Eq. (3), it is possible to perform crack growth simulations to account for CCF loading conditions. Four types of CCF crack growth tests were then performed to check the validity of the present propagation model (Fig. 7). The experiments were performed with a uniaxial Rumul machine with a load capacity of 100kN. The crack growth data were acquired using the replica technique. At specific test interruptions, a thin foil of acetate was applied to the specimen surface in correspondence of the micro-notch and acetone was dropped to allow the melting of the acetate foil into the crack. Once dried, the replica is observed under an optical microscope. Three types of load spectra were adopted:

- 1 mission corresponds to one major cycle at R = 0 and 10^2 R = 0.5 cycles (Fig. 7a).
- 1 mission corresponds to one major cycle at R = 0 and 10^3 R = 0.5 cycles (Fig. 7b).
- 1 mission corresponds to one major cycle at R = 0 and 10^4 R = 0.5 cycles (Fig. 7c).

The reported crack length corresponds to half of the total distance between the surface crack tips projected in the horizontal direction (perpendicular ot the load axis). The CCF tests reported in Fig. 7 refer to two different initial micro-notch dimensions: a = 150 μm ($\sqrt{area}$ = 187 μm) and a = 500 μm ($\sqrt{area}$ = 626 μm). Along with the experimental data, the crack growth simulations performed with a numerical integration of the Nasgro Eq. 3 are also reported. The starting crack size for the simulations was chosen according to the first crack advancement detected by the replica technique.

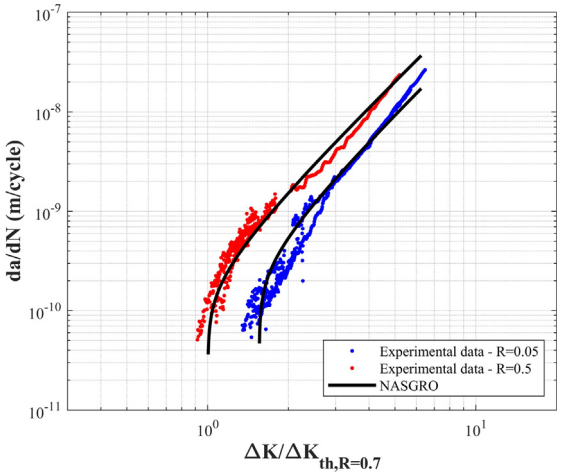

Fig. 6. Crack growth data at R = 0.5 and R = 0.05 and fitting with the Nasgro equation.

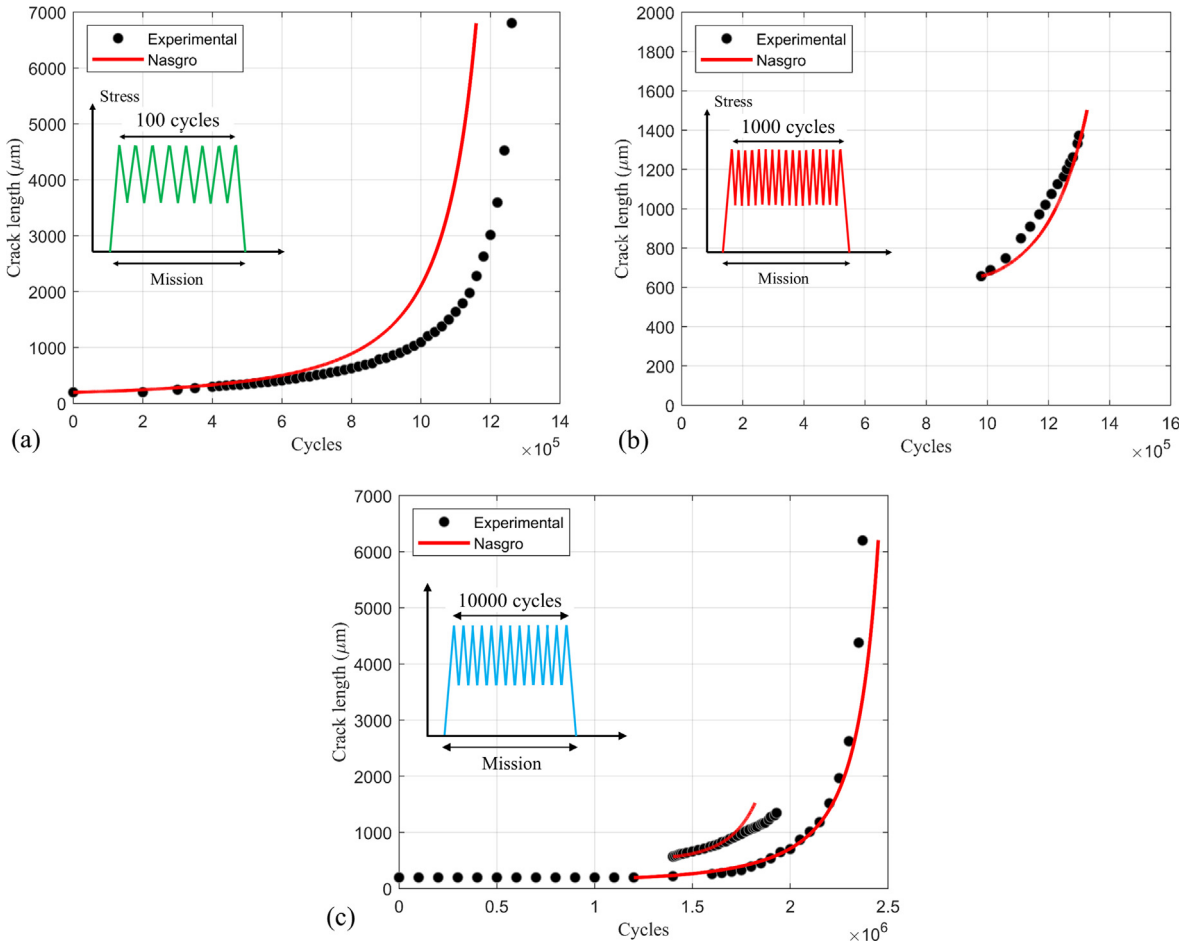

Fig. 7. CCF crack growth experiments and comparison with the simulations performed according the numerical integration of the Nasgro equation: (a) 1 mission (R = 0) performs one block of 10^2 high frequency cycles (R = 0.5) for the initial defect size equal to $\sqrt{area}$ = 187 μm, (b) 10^3 cycles at R = 0.5 for $\sqrt{area}$ = 187 μm, and (c) 10^4 high frequency cycles; this load spectra was adopted for two tests which considered the two micro-notch sizes of $\sqrt{area}$ = 187 μm and $\sqrt{area}$ = 626 μm.

3. Statistical scatter of the material properties

In this section, the scatter of the material properties derived from the experiments previously depicted is analyzed in view of the probabilistic methodology successively adopted. The probabilistic algorithm developed is based on the damage tolerance approach which accounts for the presence of a defect from which a crack is nucleated. The defect dimensions herein considered are $\sqrt{area}$ = 187 μm (short-crack regime) and $\sqrt{area}$ = 626 μm (long crack regime) which simulate, respectively, a potential crack originated from the microstructure and a crack nucleated after the impact of a foreigner object. To define a proper design methodology for the complex scenario of the CCF, it is important to analyze the variability of the endurance limits for both the short and long crack regimes. In this work, the material parameter that characterizes the long crack regime is the long crack threshold $\Delta K_{th,LC}$. The scatter of $\Delta K_{th,LC}$ depends on the load ratio and this is analyzed in the next Section 3.1. The scatter in the short-crack regime is studied according the Kitagawa-Takahashi diagram. As previously introduced, the El-Haddad model provides an analytical description of the crack size dependence of the endurance limit $\Delta\sigma_w$ based on $\Delta\sigma_{w0}$ and $\Delta K_{th,LC}$ (see Eq. (1)). To calculate the scatter of $\Delta\sigma_w$ it is then important to study the variability and the level of correlation between $\Delta\sigma_{w0}$ and $\Delta K_{th,LC}$. As it is discussed in the following, the resulting probabilistic Kitagawa-Takahashi diagrams (Section 3.2) will be used to define the design stress (Section 4).

3.1. Statistical analysis of $\Delta K_{th,LC}$

The Nasgro Eq. (3) includes the load ratio dependence of $\Delta K_{th,LC}$ which is provided explicitly with the following equation for positive load ratio [16]:

$$\Delta K_{th,LC} = \Delta K_1^* \frac{\left[\frac{1-R}{1-f}\right]^{1+RC_{th}^p}}{(1-A_0)^{(1-R)C_{th}^p}} \tag{4}$$

$$\Delta K_1^* = \Delta K_1 \sqrt{\frac{a}{a+a_0}} \tag{5}$$

ΔK_1 is the $\Delta K_{th,LC}$ as R→ 1 and it is one of the parameters to fit, C_{th} is an empirical constant with different values for positive (superscript p) and negative (superscript m) load ratios R and it is required to be fitted too. The probabilistic model relies upon the fitting procedure applied to the parameters ΔK_1 and C_{th}^p. a_0 is the El-Haddad parameter set to ~25 μm (for the present steel) and it is used in conjunction with a to account for the short-crack effect on the threshold. For the present analysis, since the fitting is performed using the experimental data obtained in the case of long cracks, a is supposed to be ~12 mm which, basically, implies that $\sqrt{\frac{a}{a+a_0}} \to 1$. The term f incorporates the crack closure effect that depends on the stress ratio R, the calculation of f is provided by the following [26]:

$$f = \frac{K_{op}}{K_{max}} = \begin{cases} max(R; A_0 + A_1 R + A_2 R^2 + A_3 R^3), & \text{se} R \geq 0 \\ A_0 + A_1 R, & \text{se} -2 \leqslant R < 0 \\ A_0 - 2A_1, & \text{se} R < -2 \end{cases} \tag{6}$$

$$A_0 = \left(0.825 - 0.34\alpha + 0.05\alpha^2\right)\left[cos\left(\frac{\pi\sigma_{max}}{2\sigma_F}\right)\right]^{1/\alpha} \tag{7}$$

$$A_1 = \left(0.415 - 0.071\alpha\right)\frac{\sigma_{max}}{\sigma_F} \tag{8}$$

$$A_2 = 1 - A_0 - A_1 - A_2 \tag{9}$$

$$A_3 = 2A_0 + A_1 - 1 \tag{10}$$

where typical input parameters are $\alpha = 2.5$ for plane strain conditions and $\sigma_{max}/\sigma_F = 0.3$. It is important to remark that the values chosen for α and σ_{max}/σ_F refer to the specific constrain conditions and material properties of the crack growth tests used to establish $\Delta K_{th,LC}$. For the specific specimen geometry adopted (Fig. 2d), it can be assumed that the plain strain condition characterizes most of the crack front and this corresponds to the choice of selecting $\alpha = 2.5$ (in the case of plane stress the parameter should be fixed equal to $\alpha = 1.0$). The second parameter is represented by the ration between the maximum (nominal) stress σ_{max} and the flow stress σ_F which is the average between the ultimate and yield stress. f can be considered constant for values of $\sigma_{max}/\sigma_F = 0.3$ or lower, we then set this parameter to 0.3 during the fitting. The adoption of Eqs. (6)–(10) for other conditions (constraint and material) should consider a proper calculation of these parameters. The fitting procedure is implemented according to the minimization of the sum of the square differences between the logarithmic experimental $\Delta K_{th,LC,exp,i}$ and the model $\Delta K_{th,LC,mod,i}$ thresholds. Accordingly, Eq. 4 can be re-written in terms of $\log_{10}$ elements as:

$$\underbrace{\log_{10}(\Delta K_{th,LC})}_{Probabilistic} = \underbrace{\log_{10}(\Delta K_1^*)}_{Probabilistic} + \underbrace{\log_{10}\frac{\left[\frac{1-R}{1-f}\right]^{1+RC_{th}^p}}{(1-A_0)^{(1-R)C_{th}^p}}}_{Deterministic} \tag{11}$$

where the deterministic component of ΔK_1^* represented by the El-Haddad correction (Eq. 5) can be incorporated in the overall deterministic term which is indicated as a constant in the following:

$$\underbrace{\log_{10}(\Delta K_{th,LC})}_{Probabilistic} = \underbrace{\log_{10}(\Delta K_1)}_{Probabilistic} + \underbrace{\log_{10}(const)}_{Deterministic} \tag{12}$$

The $i-_{th}$log-error minimization component is provided by:

$$E_i = [\log_{10}(\Delta K_{th,LC,exp,i}) - \log_{10}(\Delta K_{th,LC,mod,i})]^2 \tag{13}$$

The standard deviation related to the log-normal threshold variable can be calculated as:

$$\sigma_{\log_{10}\Delta K_1} = \sqrt{\frac{\sum E_i}{N}} \tag{14}$$

Table 3
Coefficients of variation for the $\Delta K_{th,LC}$ data fitting with Eq. 4.

least square error Batch 1 + 2	log-least square error Batch 1 + 2	log-least square error Batch 1
$CV_{\Delta K_1} = 14.3\%$	$CV_{\Delta K_1} = 10.4\%$	$CV_{\Delta K_1} = 5.5\%$

The choice to assume the $\Delta K_{th,LC}$ to be log-normally distributed implies that the confidence bands plotted in the standard coordinates depict a variability of the $\Delta K_{th,LC}$ that decreases with increasing R. This has been proven to be consistent with the fact that at lower R the crack closure greatly influences the crack driving force providing a source of scatter in the $\Delta K_{th,LC}$, while for $R \simeq 0.7$ the scatter in the $\Delta K_{th,LC}$ is not correlated with the crack closure. Therefore the logarithmic least square error fitting procedure seems to be the proper mathematical model accounting for crack closure effect over different R and moreover it provides much lower scattered data over ΔK_1 with respect to the least square error approach (see Table 3). Table 3 reports the coefficients of variance (CVs) considering two different sets of experimental results obtained from a combination of two different material batches which correspond to two different positions of the primary component. It is important to notice that when both the batches are considered, the CV increases from 5.5% to 10.4% and this influences the determination of the design stress. For this reason, both the values were considered in this study and a final comparison considering the two different CVs for the ΔK_1 variable is also provided.

Fig. 8 shows the results of the fitting procedure. Once the threshold fitting parameters were determined they can be plugged in the NASGRO model (Eq. (3)) thus describing the proper crack growth rate behavior of the material.

3.2. Probabilistic Kitagawa diagram

To define the defect tolerance maps using a probabilistic framework, the El-Haddad model previously introduced (Eq. (1)) is analyzed based on the probabilistic approach. The variables used in the El-Haddad model are the long crack threshold $\Delta K_{th,LC}$ and the endurance limit for the smooth specimens $\Delta\sigma_{w0}$. Generally speaking, these variables can be considered as independent variables or a certain level of correlation between them can be introduced. To quantify the level of variable correlation we introduce the coefficient of correlation ρ between $\Delta K_{th,LC}$ and $\Delta\sigma_{w0}$. According to the scalar value of ρ, the variables can be considered as perfectly correlated when $\rho = 1$. This conditions implies that for high values of $\Delta\sigma_{w0}$, also the values of the variable $\Delta K_{th,LC}$ are high as well. Physically, this means to consider that a material with an high endurance limit is characterized with a high resistance to crack growth rate: the main implication is that the parameter $\sqrt{area}_o$ is constant (as adopted in [10,11]). In the case of $\rho = 0$ the variables are considered completely independent [12,27,28]. The last scenario considers the variables as anti-correlated. To introduce the potential anti-correlation between $\Delta K_{th,LC}$ and $\Delta\sigma_{w0}$, we notice that $\Delta\sigma_{w0}$ is strictly related with the yield stress σ_y. To relate the literature data with the present analysis, we first notice that, for ferritic steels, the long crack threshold is proportional to the yield stress and the square-root of the grain size d as $\Delta K_{th,LC} \propto \sigma_y \sqrt{d}$ [13]. However, the yield stress and the grain size are generally anti-correlated which might determine a change in the relation between $\Delta K_{th,LC}$ and σ_y. Similar considerations can be derived for pearlitic steels for which no significant correlation between $\Delta K_{th,LC}$ and σ_y was observed. On the other side, Suzuki and McEvily studied duplex microstructures in low carbon steels and showed a direct correlation between $\Delta K_{th,LC}$ and σ_y [14], similar data can be found in [15]. Finally, for martensitic steels an anti-correlation can be observed between $\Delta K_{th,LC}$ and σ_y. This overview aims to highlight the importance to study the level of correlation between the two variables which might impart an influence in the subsequent definition of the design stress level based on the probabilistic methodology. To properly define the correlation matrix in the case of anti-correlated variables, literature data were collected for $\Delta K_{th,LC}$ and σ_Y values for martensitic steels, see Fig. 9, the data were obtained from [29,30].

From the literature data introduced, a correlation 2x2 matrix is defined in the case of anti-correlation:

$$\rho = \begin{bmatrix} 1 & -0.87 \\ -0.87 & 1 \end{bmatrix} \tag{15}$$

According to the level of correlation, the Kitagawa diagram depicted with the El-Haddad Eq. (1) changes its shape, and this can be analyzed in terms of the parameter $\sqrt{area_0}$ (Eq. (2)). The overview of this analysis is provided in Fig. 10. According to the anti-

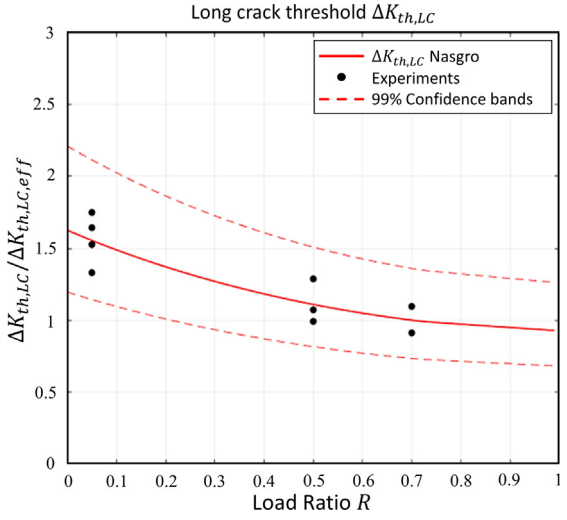

Fig. 8. Long crack thresholds as a function of the load ratio and 99% confidence bands.

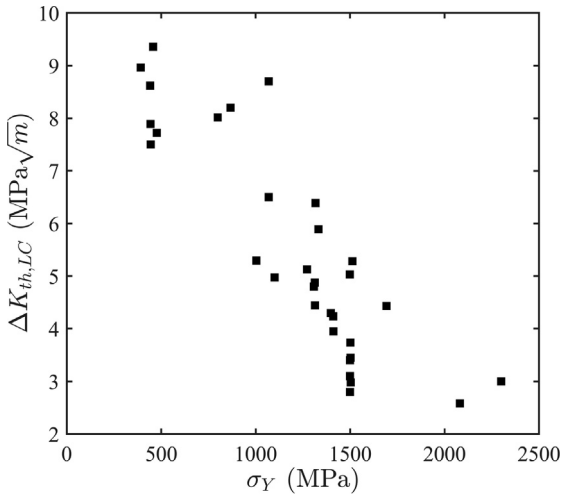

Fig. 9. $\Delta K_{th,LC}$ and σ_Y according the data for martensitic steels [29,30].

correlation hypothesis, the value of ρ introduced in the matrix defined in Eq. (15) determines the dispersion of the points extracted from the log-normal distributions of $\Delta\sigma_{w0}$ and $\Delta K_{th,LC}$ (Fig. 10a). The resulting Kitagawa diagrams show that at higher $\Delta K_{th,LC}$ the curve flattens to lower $\Delta\sigma_{w0}$ for small defects and the opposite occurs for low $\Delta K_{th,LC}$. This results in an overlap of the curves in the short crack regime which, in turn, yields a large variability of $\sqrt{area_0}$ and low scattered endurance limits in the short crack regime. The perfect correlation between $\Delta\sigma_{w0}$ and $\Delta K_{th,LC}$ results in linearly distributed extracted values from the log-normal distributions (Fig. 10c). Accordingly, the El-Haddad equation is shifted upward when the couple of extracted values are taken from the top-right of Fig. 10c, while the downward shifting occurs for low values of $\Delta\sigma_{w0}$ and $\Delta K_{th,LC}$. As a third hypothesis, the variables $\Delta\sigma_{w0}$ and $\Delta K_{th,LC}$ were assumed to be completely independent (Fig. 10e). To comment on these results it is important to notice that the most appropriate assumption on the variable correlation depends on the specific design requirements, i. e. the defect size considered. To provide a comprehensive analysis, in the following the results will be analyzed in view of all the three assumptions.

The stochastic variables considered in this study are summarized in Table 4. The CVs values obtained from the ΔK_1 and C variables were calculated from the present experimental campaign, while for C the indications by FAA were taken [31]. The scatter of the design stress ΔS was considered as the uncertainty of the local stress applied in a given point of a compressor blade [3,32,33]. Finally, the CV value for $\Delta\sigma_{w0}$ was calculated considering that the CV from the fatigue tests was approximately 5%. However, from the Haigh diagram reported in Fig. 3, it evident that $\Delta\sigma_{w0}$ is controlled by the yield stress. To account for an additional variability of $\Delta\sigma_{w0}$ determined by the batch-to-batch scatter, an additional contribution on the CV was considered based on the yield stress. From the material acceptance criteria it was estimated a CV = 5% for the batch-to-batch scatter of the yield stress. Combining the two contributions according $CV = \sqrt{CV^2_{\Delta\sigma_{w0}} + CV^2_{batch}}$ the resulting CV for $\Delta\sigma_{w0}$ is approximately 7%.

A further analysis of the simulated Kitagawa diagrams can be performed observing the normal probability plots of the $\sqrt{area_0}$ parameter of the El-Haddad model (Fig. 11) reported for both the stress ratio R = 0 and R = 0.5. For both the stress ratio it is evident that for the perfectly-correlated variable assumption the distribution of the $\sqrt{area_0}$ parameter shows no scatter, while the other two hypothesis determine a large variability.

The dimension of the defect under investigation can be analyzed with Fig. 12. In the normal probability plots shown, the distributions of the endurance limits in terms of ΔK_{th} are reported for three defect dimensions: $\sqrt{area}$ = 50 μm, 187 μm and 626 μm. According to a very small defect/crack (Fig. 12a), the scatter on the endurance limit distribution is strictly dependent on the level of correlation between $\Delta\sigma_{w0}$ and $\Delta K_{th,LC}$.

4. Design scenario

The experimental campaign previously introduced enables to define different design approaches. The physical concept of all the scenarios is defining the design stress as a limit condition for the propagation of a crack or, alternatively, as a limit condition of the maximum allowable crack size. The simplest design scenario considers only the vibrational stresses under the assumption that the effect produced by the start ups cycles (R = 0) is negligible. This scenario 0 (Fig. 13a) is clearly un-conservative, but it is useful to be used as a reference case. A second design scenario (number 1, Fig. 13b) uses the number of target missions of the engine (number of start-ups, load ratio R = 0) to perform a calculation of the crack advancement induced only by these cycles. The advanced crack is successively used to calculate the design stress based on the Kitagawa diagram. Nevertheless this procedure is a simplification of the real load history, it considers the load cycles at R = 0 and it allows to define a simplified and computationally-efficient probabilistic framework.

The third design approach (scenario 2, Fig. 13c) performs a complete crack propagation simulation in order to determine the limit stress range required to reach a critical final crack length a_{crit}. This scenario simulates precisely the real CCF operational conditions of

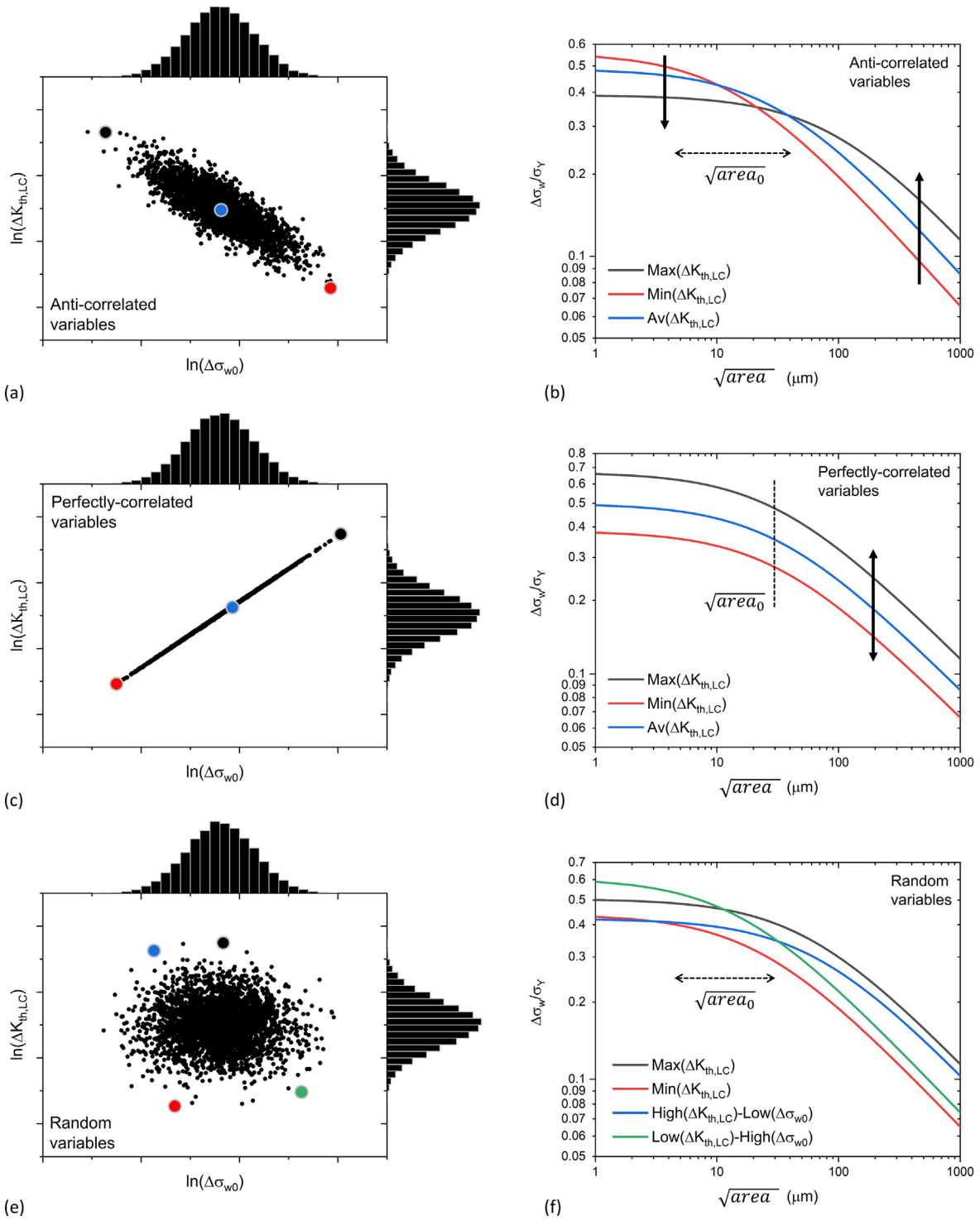

Fig. 10. Kitagawa diagrams depicted according a statistical analysis of the El-Haddad model: (a)-(b) anti correlation between $\Delta\sigma_{w0}$ and $\Delta K_{th,LC}$ determines a high scatter of the $\sqrt{area_0}$ while the (c)-(d) perfect correlation assumption results in a shifting of the curve and in a constant $\sqrt{area_0}$; finally, the (e)-(f) independent (random) assumption for $\Delta\sigma_{w0}$ and $\Delta K_{th,LC}$.

the engine and it is the most realistic between the three approaches. However, from the computational point of view, the probabilistic approach demands heavy calculations to calculate the design stress at the desired probability of failure.

The failure probability was chosen to be $P_f = 7.2{\cdot}10^{-5}$ which is consistent with the Eurocode and BS7910 standards for primary

Table 4
Values of the coefficients of variance for the stochastic variables adopted in the present study.

	Distribution	Coefficient of Variance (CV)
ΔS	gaussian	5, 10, 15%
ΔK_1	log-normal	5.5, 10.4%
$\Delta\sigma_{w0}$	log-normal	7%
C	log-normal	7.68%

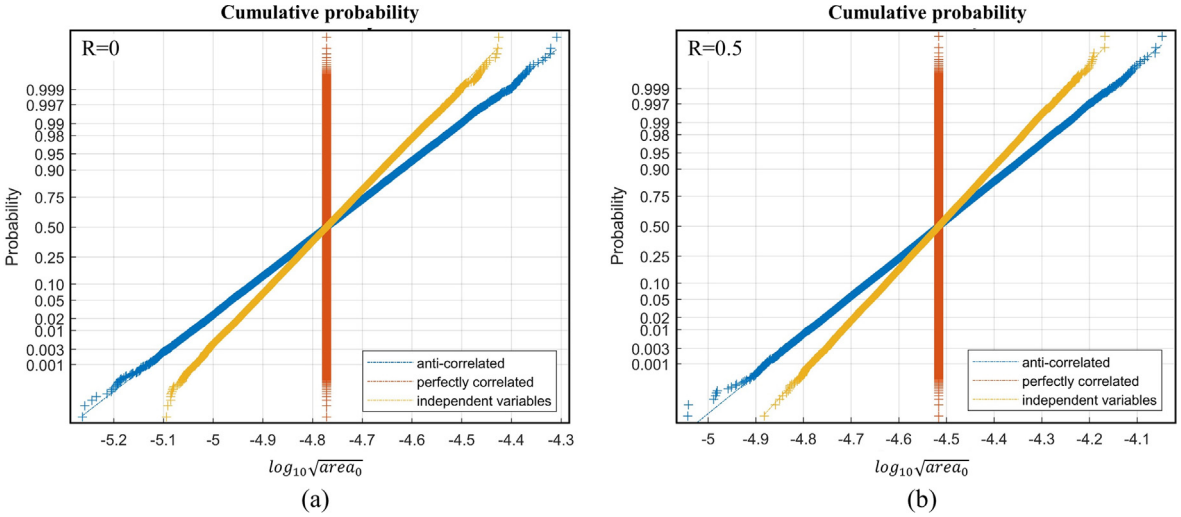

Fig. 11. Normal probability plots for the El-Haddad parameter $\sqrt{area_0}$ for the load ratio (a) R = 0 and (b) R = 0.5.

components [34,35]. As for the number of Monte Carlo simulations, they were chosen so that 95% confidence bands of the failure probability correspond to an error of ± 10% [36].

4.1. Scenario 0

The first scenario 0 analyzed is based on the definition of the design stress range ΔS_0 according a non-propagating crack for the load cycles occurring at positive load ratio $R > 0$ neglecting the major load cycles (R = 0). Even if simplified approaches (such as the *Top of Scatter* [37]) could be adopted, the calculation of ΔS_0 was carried out with Monte Carlo simulations according the following steps:

- Extraction of the random variables ΔK_1 and $\Delta\sigma_{w0}$ which can have a certain degree of correlation as depicted in the Fig. 10.
- For each Monte Carlo iteration a Kitagawa-Takahashi diagram is built according the El-Haddad model (Eq. (1)) and the previously extracted ΔK_1 (which allows to determine $\Delta K_{th,LC}$ from Eqs. 4 and 5) and $\Delta\sigma_{w0}$.
- At each iteration, a value of $\Delta\sigma$ is extracted from the distribution of the applied stress rage (mean value ΔS and coefficient of variance $CV_{\Delta S}$) and failure occurs when

$$\Delta\sigma > \Delta\sigma_w = \Delta\sigma_{w0}\sqrt{\frac{\sqrt{area_0}}{\sqrt{area} + \sqrt{area_0}}} \tag{16}$$

- The algorithm is repeated iteratively according the average value of the applied stress range ΔS until the probability of failure defined as

$$P_f = Pr[\Delta\sigma > \Delta\sigma_w] \rightarrow P_f = Pr\left[I = \frac{\Delta\sigma_w}{\Delta\sigma_{w0}} > \sqrt{\frac{\sqrt{area_0}}{\sqrt{area} + \sqrt{area_0}}}\right] \tag{17}$$

reaches $P_f = 7.2{\cdot}10^{-5}$.

4.2. Scenario 1

The design scenario 1 accounts for the effect of the startup cycles (R = 0). The crack advancement induced by the startup cycles is simulated as the cycles occur consecutively. This simplification aims to reduce the computational time for the probabilistic

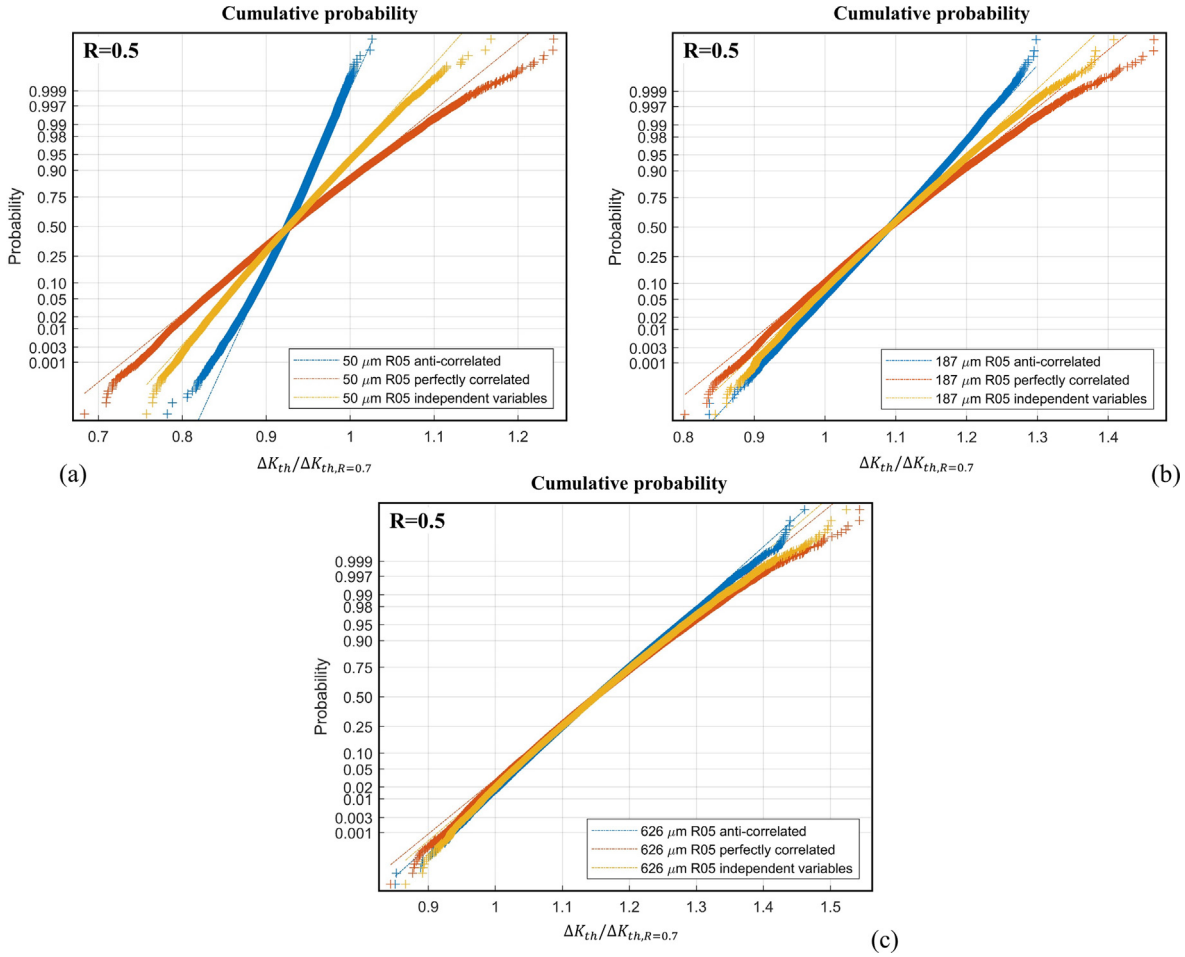

Fig. 12. Normal probability plots of the endurance limits calculated in terms of ΔK_{th} for (a) $\sqrt{area} = 50\ \mu m$, (b) $\sqrt{area} = 187\ \mu m$ and (c) $\sqrt{area} = 626\ \mu m$.

assessment framework implementation. The advanced crack is then analyzed according to the same procedure previously discussed for the Scenario 0. The difference is that the crack size used to calculate the design stress ΔS_1 (herein defined according the subscript 1 to relate it with the scenario 1) using the El-Haddad model is not fixed but it is characterized by a statistical distribution due to the variability introduced for the variables C and ΔK_1. The steps for the implementation of the Monte Carlo simulation are the following:

- The stress range $\Delta S^{R=0}$ for the major cycles (R = 0) is used to calculate the crack advancement considering $N_1^{R=0}$ cycles:

$$a_f = \int_0^{N_1^{R=0}} f(a, \Delta K^{R=0}, \Delta K_{th,LC}) da \tag{18}$$

  $f(a, \Delta K^{R=0}, \Delta K_{th,LC})$ is the Nasgro equation used for R = 0 and $\Delta K^{R=0} = F \cdot \Delta S^{R=0} \sqrt{pi \cdot a}$; F represents the geometrical factor.
- The loading cycles at positive load ratio (in the present case R = 0.5) determine a stress range equal to $\Delta S^{R>0} = (1 - R)\Delta S^{R=0}$ which results in a SIF range of:

$$\Delta K = F \cdot \Delta S^{R>0} \sqrt{\pi \cdot a_f} \tag{19}$$

- The failure probability is calculated according:

$$P_f = Pr[\Delta K > \Delta K_{th,SC}] \tag{20}$$

  $\Delta K_{th,SC}$ is the threshold SIF range for short cracks determined from the Kitagawa diagram with the El-Haddad Eq. (1) written in terms of SIF range:

$$\Delta K_{th,SC} = \Delta K_{th,LC} \cdot \sqrt{\frac{\sqrt{area}}{\sqrt{area + \sqrt{area_0}}}} \tag{21}$$

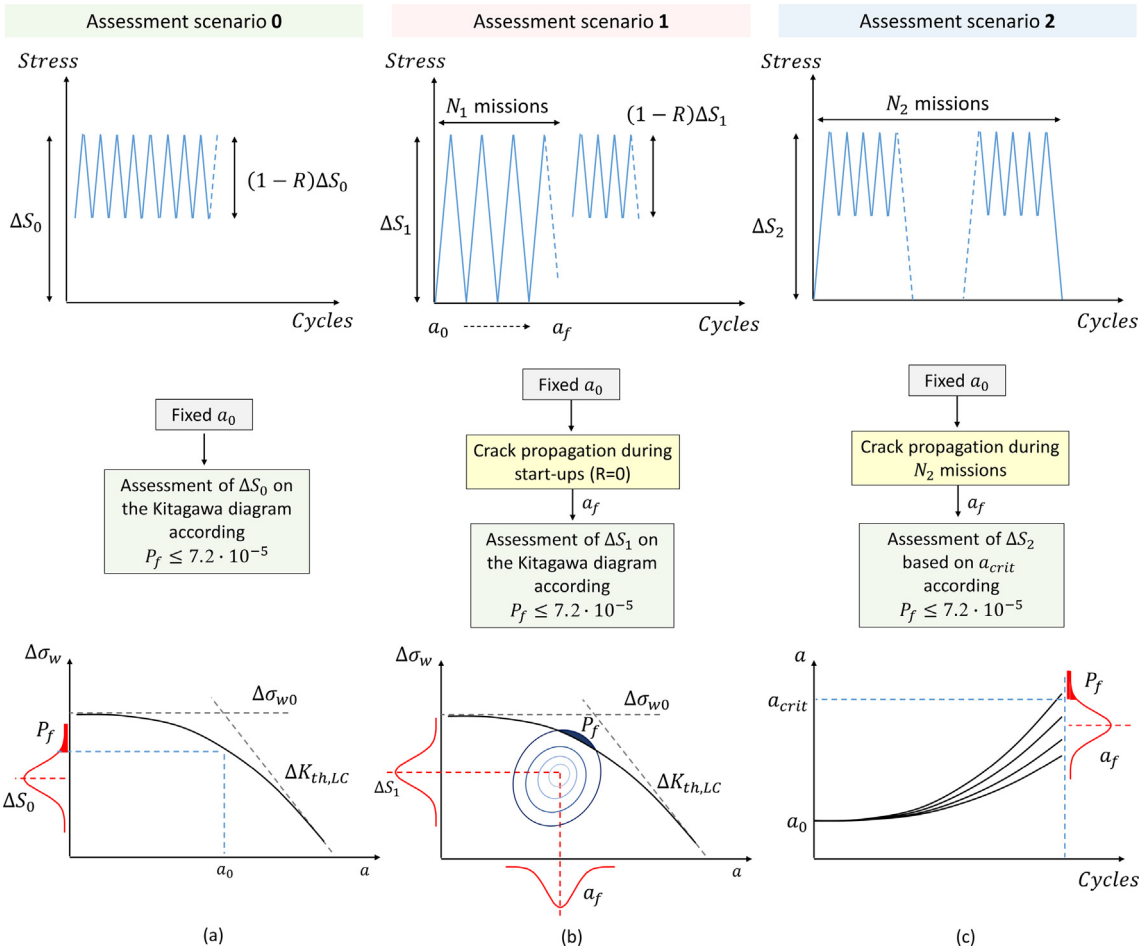

Fig. 13. The design scenario implemented in this study: (a) the design stress range is defined according a non-propagating short crack under the high frequency cycles at R = 0.5 (scenario 0), (b) the design stress range is defined accounting an advanced short crack under the target operational R = 0 cycles (scenario 1), (c) the design stress range considers a maximum critical crack size (scenario 2).

Combining Eqs. (20) and (21) it is possibile to write the failure condition as:

$$P_f = Pr\left[I = \frac{\Delta K}{\Delta K_{th,LC}} > \sqrt{\frac{\sqrt{area}}{\sqrt{area} + \sqrt{area_0}}}\right] \tag{22}$$

I indicates a failure index. Providing Eqs. (18), (19) and (21), a Monte Carlo simulation tool was implemented to define a design stress range ΔS_1 such that the probability of failure determined for the failure index I converges to $P_f = 7.2{\cdot}10^{-5}$. The analyses were performed with a fixed initial defect size of $\sqrt{area} = 187\ \mu m$ and a number of start-ups cycles $N_1 = 18,000$ which represents a severe service of 30 years.

4.3. Scenario 2

According to Fig. 13c, the scenario 2 aims to simulate precisely the crack advancement induced by the real CCF conditions. In particular, scenario 2 is an improvement of scenario 1. The crack propagation is implemented considering the sequential repetition of the gas turbine operating cycle composed of a single startup (major load cycle at R = 0) and 10^4 R = 0.5 vibrational stress cycles. It's the most realistic condition reflecting the effective material behavior. However, the huge number of iterations leads to very long computational time when the simulation is coupled with the probabilistic methodology. The NASGRO equation was used to simulate the crack development to a fixed final crack length a_f:

$$a_f = \int_0^{N_f} f(a, \Delta K, \Delta K_{th,LC}, \sqrt{area_0}_{R=0}, \sqrt{area_0}_{R=0.5}) da \tag{23}$$

where ΔK is determined from the iterative applied stress range according $\Delta K = F\Delta S\sqrt{\pi a}$. $\sqrt{area_0}_{R=0}$ and $\sqrt{area_0}_{R=0.5}$ are the El-Haddad constants for the load cycles R = 0 and R = 0.5, respectively. These material properties are considered stochastic variables

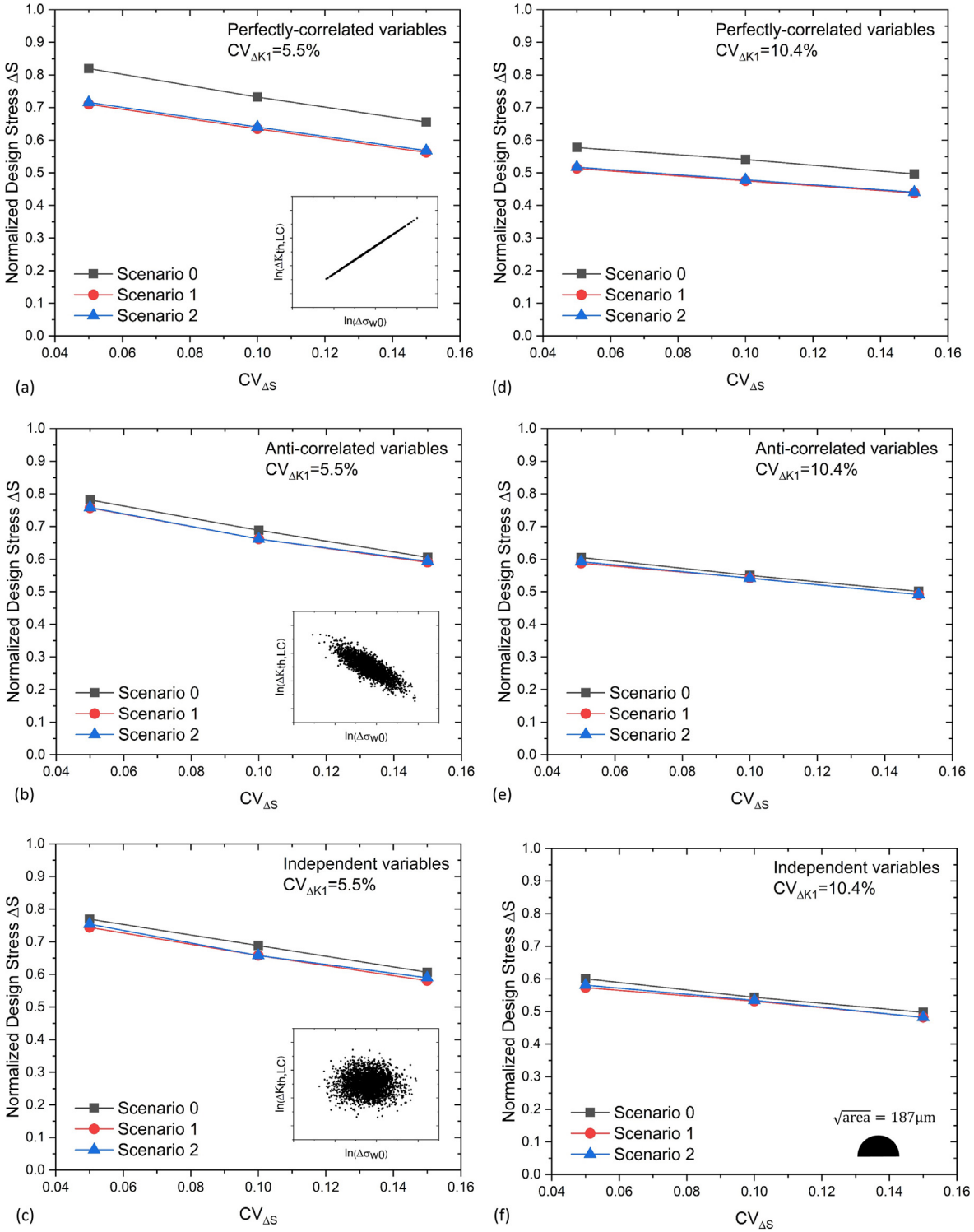

Fig. 14. Normalized design stress ranges ΔS ($\Delta S_i/\Delta S_{0,det}$ with i = 0, 1, 2) simulated according the CV reported in the Table 4. (a)–(c) illustrates the results considering $CV_{\Delta K_1}$ = 5.5%, while (d)–(f) shows the results for $CV_{\Delta K_1}$ = 10.4%. The figures differentiate according the level of correlation between the variables $\Delta\sigma_{w0}$ and ΔK_1.

in the present calculation as their dependence on the iterative ΔK_1 and $\Delta\sigma_{w0}$. The simulations were performed to acquire ΔS_2-P_f data. Successively, these points were fitted to determine the design stress ΔS_2 at $P_f = 7.2{\cdot}10^{-5}$.

5. Results and discussion

The design stress ranges $\Delta S_{0,1,2}$ were calculated implementing the algorithms depicted in the previous section according the CVs of the stochastic variables introduced in Table 4. The summary of the results for all the cases analyzed is shown in Fig. 14. The results were normalized according to the design stress $\Delta S_{0,det}$ calculated according the scenario 0 for the case of deterministic variables, i.e. using the mean value.

Figs. 14a–c show the simulations performed with the assumption of low scattered $\Delta K_{th,LC}$ values which results in $CV_{\Delta K_{th,LC}} = 5.5\%$, while the Figs. 14d-f indicate the $CV_{\Delta K_{th,LC}} = 10.4\%$. In general, a higher uncertainty of the stresses of the component and a higher $CV_{\Delta S}$ results in a decrease of the allowable design stress ΔS. This effect can be quantified as the decrease of the design stress range is approximately 10% when the $\mathrm{CV}_{\Delta S}$ changes from 5% to 15%. One of the most significant result can be better analyzed in the summary of the results presented in Fig. 15. According the case of $\mathrm{CV}_{\Delta K_1} = 5.5\%$ (Fig. 15a), it can be observed that the three different hypotheses on the correlation between the endurance limit $\Delta\sigma_{w0}$ and the long crack threshold parameter ΔK_1 do not have a paramount influence on the final design stress.

Considering the design scenario, as expected the scenario 0 is not conservative, while the scenario 1 and 2 determine basically the same outcome. The analyses performed adopting $\mathrm{CV}_{\Delta K_1} = 10.4\%$ provide a general decrease of the design stress, this is of particular importance as the defect length under investigation is close to the region dominated by the long crack behavior, then it is expected that the variability of the stochastic variable ΔK_1 profoundly influences the design stress. The same variable is also responsible of the small difference between the design stresses predicted by the scenario 1 and 2 (Fig. 15b). However, the main outcome of these results is that the design scenario 1, although represents a simplification of the damage process, leads to the same results as the scenario 2. Its main advantage is that the calculation time is much shorter (in a ratio 1: 30) than to the one of Scenario 2.

6. Concluding remarks

The present work proposes a probabilistic analysis to determine the design stress for a component subjected to combined cycle fatigue in the framework of a damage tolerance design. An extensive experimental campaign was initially performed to determine the material properties in terms of long crack thresholds, endurance limits for smooth specimens, endurance limits for micro-notched specimens and fatigue crack growth rates for the load ratio R = 0 (representing the startup cycle of the component) and R = 0.5 (vibrational stresses superimposed to the major loading cycles). Based on the scatter of the material properties and the adoption of the El-Haddad model to describe the endurance limit as a function of the defect dimension, three different design scenario were implemented according different level of physical description of the fatigue damage process. Based on the results presented, the subsequent conclusions are proposed:

- Scenario 0 is purely based on the non-propagation of the initial defect and then it is non-conservative respect to the other design criteria.
- Scenario 2 simulates the crack propagation under the real combined cycle fatigue conditions; it is the most accurate algorithm providing a lower design stresses respect to Scenario 0. However, the implementation of the algorithm, for the different

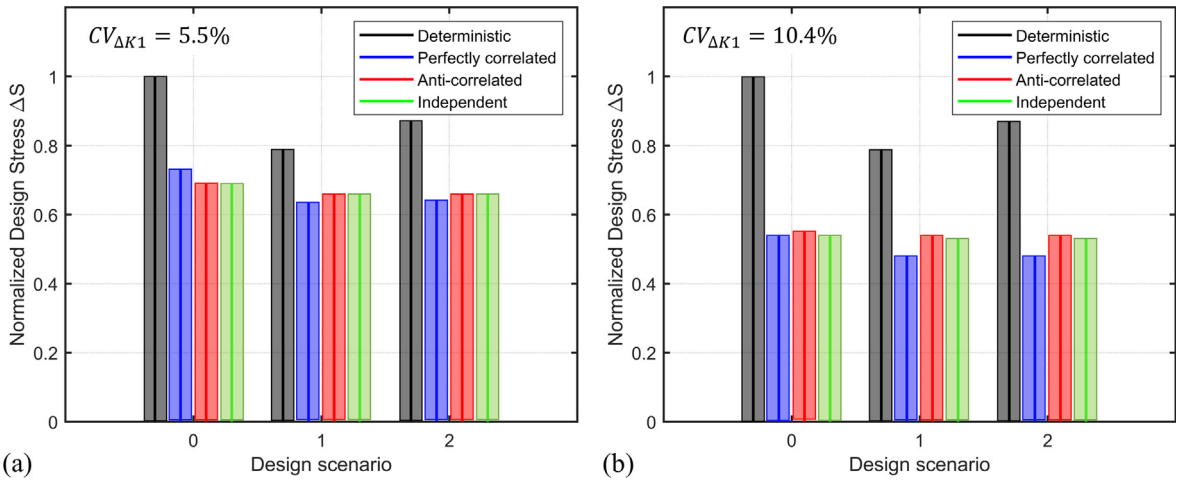

Fig. 15. Comparison between the normalized design stress ranges ΔS ($\Delta S_i/\Delta S_{0,det}$ with $i = 0, 1, 2$) calculated assuming two coefficients of variance for the ΔK_1 parameter: (a) $\mathrm{CV}_{\Delta K_1} = 5.5\%$, b) $\mathrm{CV}_{\Delta K_1} = 10.4\%$, the calculations were performed considering $\sqrt{area} = 187\ \mu\mathrm{m}$, $\mathrm{CV}_{\Delta S} = 10\%$, $\mathrm{CV}_{\Delta\sigma_{w0}} = 7\%$ and $\mathrm{CV}_{log,C} = 7.68\%$. The deterministic solution for the scenario 0 is selected as the reference assessment scenario.

probabilistic models of the Kitagawa diagram, has an important computational effort.

- Scenario 1 simplifies the design approach accounting only for the crack advancement induced by the major cycles and calculating successively the design stress from the El-Haddad model obtained for the vibrational stresses. It is as accurate as Scenario 2 with a computational time which is approximately 30 times less.

Declaration of Competing Interest

The authors declare that they have no known competing financial interests or personal relationships that could have appeared to influence the work reported in this paper.

Acknowledgements

The activity was carried out within the H2020 Project Flexturbine (Grant n. 653941). The authors acknowledge permission by the Flexturbine Consortium to publish the present paper.

References

[1] Reed RC. The superalloys: fundamentals and applications. Cambridge University Press; 2008.
[2] Boyd-Lee A, Harrison G, Henderson M. Evaluation of standard life assessment procedures and life extension methodologies for fracture-critical components. Int J Fatigue 2001;23:11–9.
[3] Wu Y, Enright M, Millwater H. Probabilistic methods for design assessment of reliability with inspection. AIAA J 2002;40(5):937–46.
[4] Leverant G, Millwater H, McClung R, Enright M. A new tool for design and certification of aircraft turbine rotors. J Eng Gas Turbines Power 2004;126:155–9.
[5] McClung R, Enright M, Millwater H, Leverant G, Hudak S. A software framework for probabilistic fatigue life assessment of gas turbine engine rotor. J ASTM Int 2004;1(8).
[6] Beretta S, Foletti S, Madia M, Cavalleri E. Structural integrity assessment of turbine discs in presence of potential defects: probabilistic analysis and implementation. Fatigue Fract Eng Mater Struct 2015;38(9):1042–55.
[7] Kitagawa H, Takahashi S. Applicability of fracture mechanics to very small cracks or the cracks in the early stage. In: Proc. of 2nd ICM, Cleveland, vol. 1976; 1976. p. 627–31.
[8] Zerbst U, Vormwald M, Pippan R, Gänser H-P, Sarrazin-Baudoux C, Madia M. About the fatigue crack propagation threshold of metals as a design criterion–a review. Eng Fract Mech 2016;153:190–243.
[9] El Haddad MH, Topper TH, Smith KN. Prediction of non propagating cracks. Eng Fract Mech 1979;11(3):573–84.
[10] Gagnon M, Tahan A, Bocher P, Thibault D. A probabilistic model for the onset of high cycle fatigue (hcf) crack propagation: application to hydroelectric turbine runner. Int J Fatigue 2013;47:300–7.
[11] Gagnon M, Tahan A, Bocher P, Thibault D. Influence of load spectrum assumptions on the expected reliability of hydroelectric turbines: a case study. Struct Saf 2014;50:1–8.
[12] Liu Y, Mahadevan S. Probabilistic fatigue life prediction using an equivalent initial flaw size distribution. Int J Fatigue 2009;31(3):476–87.
[13] Chan K. Scaling laws for fatigue crack. Metall Trans A 1993;24(11):2473–86.
[14] Suzuki H, McEvily A. Microstructural effects on fatigue crack growth in a low carbon steel. Metall Trans A 1979;10(4):475–81.
[15] Taylor D, Jianchung L. Sourcebook on fatigue crack propagation: thresholds and crack closure. Emas 1993.
[16] NASGRO 4.2 manual; 2006.
[17] Murakami Y, Endo M. Quantitative evaluation of fatigue strength of metals containing various small defects or cracks. Eng Fract Mech 1983;17(1):1–15.
[18] E. ASTM International, Standard practice for conducting force controlled constant amplitude axial fatigue. tests of metallic materials; 2015.
[19] ISO, Metallic materials – Fatigue testing- Statistical planning and analysis of data. 12107:2017, Tech. Rep. 0; 2017.
[20] FKM Guideline, Analytical strength assessment of components in mechanical engineering, 6th Edition, VDMA-Verl; 2012.
[21] Newman Jr JC, Raju IS. Stress-intensity factor equations for cracks in three-dimensional finite bodies subjected to tension and bending loads. NASA technical reports, NASA-TM-85793, NAS 1.15:85793; 1984.
[22] Newman Jr. J, Schneider J, Daniel A, McKnight D. Compression pre-cracking to generate near threshold fatigue-crack-growth rates in two aluminum alloys. Int J Fatigue 2005;27(10):1432–40.
[23] Carboni M, Patriarca L, Regazzi D. Determination of δk th by compression pre-cracking in a structural steel. J ASTM Int 2009;6(9):1–13.
[24] Newman Jr. J, Yamada Y. Compression precracking methods to generate near-threshold fatigue-crack-growth-rate data. Int J Fatigue 2010;32(6):879–85.
[25] E. ASTM International, Standard test method for measurement of fatigue crack growth rates; 2015.
[26] Newman Jr. J. A crack opening stress equation for fatigue crack growth. Int J Fract 1984;24(4):R131–5.
[27] Koutiri I, Bellett D, Morel F, Pessard E. A probabilistic model for the high cycle fatigue behaviour of cast aluminium alloys subject to complex loads. Int J Fatigue 2013;47:137–47.
[28] Le V-D, Morel F, Bellett D, Saintier N, Osmond P. Simulation of the kitagawa-takahashi diagram using a probabilistic approach for cast al-si alloys under different multiaxial loads. Int J Fatigue 2016;93:109–21.
[29] Taylor D. Fatigue thresholds: their applicability to engineering situations. Int J Fatigue 1988;10(2):67–79.
[30] Taylor D, Jianchung L. Sourcebook on fatigue crack propagation: thresholds and crack closure. Emas 1993.
[31] Federal Aviation Administration, Damage Tolerance Assessment Handbook; 1993.
[32] Schönbauer BM, Stanzl-Tschegg SE, Perlega A, Salzman RN, Rieger NF, Zhou S, et al. Fatigue life estimation of pitted 12% cr steam turbine blade steel in different environments and at different stress ratios. Int J Fatigue 2014;65:33–43.
[33] Härkegård G. Short-crack modelling of the effect of corrosion pits on the fatigue limit of 12% cr steel. Fatigue Fract Eng Mater Struct 2015;38(9):1009–16.
[34] U. Standard, Eurocode 0 – basis of structural design; 2006.
[35] Publication BS. Guide to methods for assessing the acceptability of flaws in metallic structures; 2013.
[36] Mahadevan S, Haldar A. Probability, reliability and statistical method in engineering design. John Wiley & Sons; 2000.
[37] Tong YC. Literature review on aircraft structural risk and reliability analysis, Tech. rep., Defence science and technology organisation Melburne (Australia); 2001.